nature portfolio

https://doi.org/10.1038/s41592-021-01154-y

Supplementary information

A pairwise distance distribution correction (DDC) algorithm to eliminate blinking-caused artifacts in SMLM

In the format provided by the authors and unedited

Supporting Material for: A Pairwise Distance Distribution Correction (DDC) algorithm to eliminate blinking-caused artifacts in SMLM

Christopher H. Bohrer[1, 3], Xinxing Yang[1], Shreyasi Thakur[4], Xiaoli Weng[1], Brian Tenner[2], Ryan McQuillen[1], Brian Ross[2], Matthew Wooten[5], Xin Chen[5], Jin Zhang[2], Elijah Roberts[3], Melike Lakadamyali[4], and Jie Xiao[1]

[1] Department of Biophysics and Biophysical Chemistry, Johns Hopkins School of Medicine

[2]Department of Pharmacology, University of California, San Diego

[3]Department of Biophysics, Johns Hopkins University

[4]Department of Physiology, Perelman School of Medicine, University of Pennsylvania

[5]Department of Biology, Johns Hopkins University

Contents

1 Tables Giving Brief Overview of Field

Table 1:

Method	Operating principle and note	Require additional Experiments ?	Accounts for Localization Error?	Use of Time Domain?	Utilizes Information About True Distribution of Fluorophores?	Result in a Corrected Image?
DDC	Utilizes the true pairwise distance distribution to define a likelihood, which when maximized will result in a corrected image.	No	Yes	Yes	Yes	Yes
Betzig E, Patterson GH, Sougrat R, Lindwasser OW, Olenych S, et al. (2006) Imaging intracellular fluorescent proteins at nanometer resolution. Science 313: 1642–1645.	With the development of SMLM, overcounting was immediately recognized as a problem. To account for this arbitrary time and distance thresholds were chosen to result in a corrected image.	No	Yes	Yes	No	Yes
Annibale, P., Vanni, S., Scarselli, M., Rothlisberger, U., Radenovic, A., 2011. Quantitative photo activated localization microscopy: unraveling the effects of photoblinking. PLoS One 6 (7), e22678.	Utilizes a semi-empirical formula to estimate the photokinetics of the fluorophore, which can also be used to determine a time threshold where overcounting is eliminated.	No	Yes	Yes	No	Yes
Coltharp, C., Kessler, R.P. and Xiao, J., 2012. Accurate construction of photoactivated localization microscopy (PALM) images for quantitative measurements. *PLoS One* , *7* (12), p.e51725.	Utilizes the average number of blinks per fluorophore, and scans thresholds in time and space to determine the best thresholds, which are the ones resulting in the correct number of true localizations. These thresholds are then used to create a corrected image.	Yes	Yes	Yes	No	Yes
Puchner, E.M., Walter, J.M., Kasper, R., Huang, B. and Lim, W.A., 2013. Counting molecules in single organelles with super resolution microscopy allows tracking of the endosome maturation trajectory. Proceedings of the National Academy of Sciences, 110(40), pp.16015-16020.	By quantifying the off time distribution of the fluorophore, this method sets generous thresholds to eliminate the possibility of overcounting. Specifically the time threshold is set to equal to 99% quartile for the off time distribution, which could lead to significant undercounting.	Yes	Yes	Yes	No	Yes
Fazel, M., Wester, M.J., Rieger, B., Jungmann, R. and Like, K.A., 2019. Sub-Nanometer Precision using Bayesian Grouping of Localizations. *bioRxiv* , p.752287.	Utilizes a Bayesian approach to link localizations into trajectories based on their spatial proximity, this is done by incorporating the spread of the point spread function	Depends	Yes	Only in accountin g for drift	No	Yes
Lee, S.H., Shin, J.Y., Lee, A. and Bustamante, C., 2012. Counting single photoactivatable fluorescent molecules by photoactivated localization microscopy (PALM). *Proceedings of the National Academy of Sciences*	An iterative algorithm with a calibration curve (of the best time threshold for a certain number of fluorophores) is used to quantify the number of molecules within a small field of view.	Depends	No	Yes	No	No

Method	Operating principle and note	Require additional Experiments ?	Accounts for Localization Error?	Use of Time Domain?	Utilizes Information About True Distribution of Fluorophores?	Result in a Corrected Image?
Rollins, G.C., Shin, J.Y., Bustamante, C. and Pressé, S., 2015. Stochastic approach to the molecular counting problem in super resolution microscopy. *Proceedings of the National Academy of Sciences* , *112* (2), pp.E110-E118.	Quantifies the number of fluorophores within a region of interest using different photokinetic models to determine the likelihood of having a certain number of true localizations within the target area. It also estimates for the photokinetic rates.	No	No	Yes	No	No
Sengupta, P., Jovanovic-Talisman, T., Skoko, D., Renz, M., Veatch, S.L. and Lippincott-Schwartz, J., 2011. Probing protein heterogeneity in the plasma membrane using PALM and pair correlation analysis. *Nature methods* , *8* (11), pp.969-975.	Computes the pair-correlation function and fits it to an ideal equation to determine if fluorophores are clustered and to what extent.	No	Yes	No	No	No
Veatch, S.L., Machta, B.B., Shelby, S.A., Chiang, E.N., Holowka, D.A. and Baird, B.A., 2012. Correlation functions quantify super-resolution images and estimate apparent clustering due to over-counting. *PloS one* , *7* (2), p.e31457.	Computes the pair-correlation function and fits it to an ideal equation to determine if fluorophores are clustered and to what extent. Also utilizes two-color experiments and cross-correlation to determine the extent of clustering.	No	Yes	No	No	No
Zanacchi, F.C., Manzo, C., Alvarez, A.S., Derr, N.D., Garcia-Parajo, M.F. and Lakadamyali, M., 2017. A DNA origami platform for quantifying protein copy number in super-resolution. *Nature methods* , *14* (8), p.789.	Utilizes DNA origami to quantify the distributions of number of blinks for different molecular species. These known distributions can then be used to determine the relative populations of each species in the sample.	Yes	No	No	No	No
Hummer, G., Fricke, F. and Heilemann, M., 2016. Model-independent counting of molecules in single-molecule localization microscopy. *Molecular biology of the cell* , *27* (22), pp.3637-3644.	Derived a function to describe the number of blinking events per fluorophore. This function is then used to fit the number of blink distributions, providing the proportion of molecules that are monomers, dimers, and etc.	Yes	No	No	No	No
Nino, D., Rafiei, N., Wang, Y., Zilman, A. and Milstein, J.N., 2017. Molecular counting with localization microscopy: A Bayesian estimate based on fluorophore statistics. *Biophysical Journal* , *112* (9), pp.1777-1785.	Utilizes an experimentally determined number of localizations per fluorophore to fit the number of blink distributions to determine the number of fluorophores in a certain region. Tagging a target with multiple fluorophores can dramatically decrease the error in this calculation.	Yes	No	No	No	No

Method	Operating principle and note	Require additional Experiments ?	Accounts for Localization Error?	Use of Time Domain?	Utilizes Information About True Distribution of Fluorophores?	Result in a Corrected Image?
Baumgart, F., Arnold, A.M., Leskovar, K., Staszek, K., Fölser, M., Weghuber, J., Stockinger, H. and Schütz, G.J., 2016. Varying label density allows artifact-free analysis of membrane-protein nanoclusters. Nature methods, 13(8), pp.661-664.	By experimentally varying the labeling density and imaging the same sample repeatedly one can determine if a target forms a clustered distribution or not, independent of the fluorophores blinking behavior.	Yes	No	No	No	No
Spahn, C., Herrmannsdörfer, F., Kuner, T. and Heilemann, M., 2016. Temporal accumulation analysis provides simplified artifact-free analysis of membrane-protein nanoclusters. *Nature methods* , *13* (12), pp.963-964.	Computationally varies the labeling density (similar to Baumgart et al.), to determine the extent of protein clustering.	No	No	No	No	No

2 Mathematical justification for true pairwise distance distribution

Here we provide a mathematical justification supporting the principle that the true pairwise distance distribution is obtained when the pairwise distances are taken between localizations separated by a frame difference much longer than the average lifetime of the fluorophore.

Blinking causes the position of a fluorophore to appear throughout multiple frames, we refer to the localizations from the same fluorophore as a blinking trajectory and we define the first localization in a blinking trajectory as the true localization and all subsequent localizations as repeats. An illustration of two blinking fluorophores for a one dimensional image is shown in Fig.S1 with the true localizations of the fluorophores shown as green dots and repeats in red. For this justification we assume that the blinking behavior of the fluorophores are independent of each other and the photo-kinetics of the fluorophores are constant and uniform throughout the acquisition of the image. Note: this is one of the major assumptions needed to apply DDC.

The number of repeats for an arbitrary fluorophore, a, follows an unknown random variable, $num_b(a)$, and the determination of the true position of fluorophore a, x_a, is dependent upon the localization precision of the microscope, δ. For the toy model in Fig.S1 we have no error in determining the position of the fluorophore for simplicity. The distances contributed by two arbitrary fluorophores within an image can then be split into the three arrays/categories below:

$$\left\{ \begin{array}{c} C1 = \sqrt{((x_a+\delta)-(x_b+\delta))^2} \\ C2(1:\gamma) = \sqrt{((x_a+\delta)-(x_b+\delta))^2} \\ C3(1:\gamma') \approx \sqrt{((\delta)-(\delta))^2} \end{array} \right\},$$

where $\gamma = (num_b(a) + num_b(b) + num_b(a) \times num_b(b))$ and $\gamma' = \sum_{n=0}^{num_b(a)} n + \sum_{n=0}^{num_b(b)} n$, are the number of distances contributed to the pairwise distance distribution for the different categories. Here we should note that the number of distances contributed by the repeats [C2 and C3] can be much higher than the distances contributed by the true localizations, $C1$. The pairs of localizations belonging to the three categories for the two fluorophores are shown in Fig.S1 for reference.

The distances in each of the categories are separated in time by a certain number of frames, Δn. We define

N as the maximum lifetime of a fluorophore, and can be approximated with a value that is much larger than the average lifetime of the fluorophore for real experiments (see below for further discussion).The fact that the fluorescent fluorophores have a limited lifetime creates constraints on the frame differences the distances in each category can posses. The possible frame differences for the distances in categories $C2$ and $C3$ are then the following:

$$\left\{ \begin{array}{c} \Delta n_{C1} - N < \Delta n_{C2} < \Delta n_{C1} + N \\ \Delta n_{C3} < N \end{array} \right\},$$

where Δn_{C1} is the frame difference between the true localizations in $C1$.

Notice that if we only use the distances between localizations that are separate in time by N, $\Delta n = N$, a pair of arbitrary fluorophores that have at least some localizations in their blinking trajectories with a frame difference of N will contribute a certain number of distances, from $C1$ and $C2$ and all of the distances in $C3$ will be eliminated. [Note, that for experiments N should be approximated with a value that is much larger than the average lifetime of the fluorophore — this will result in minimal error due to the nature of lifetime distributions, that is, even if N is not greater than the lifetime of every fluorophore within the image, due to the exponential shaped distributions there will be very few fluorophores with a lifetime greater. Note, see next section to get an idea as to the extent of this error. Therefore, the number of distances left within C3 will be negligible if large N are chosen].

Now, if we use the distances with $\Delta n = N$, the number of distances contributed from $C1$ and $C2$ from any pair of arbitrary fluorophores follows the unknown random variable ϕ. [The distances contributed by each pair of fluorophores follows the same unknown random variable because the photo-kinetics of each fluorophore is the same.]

Then, to obtain an accurate approximation of the true pairwise distance distribution, $P_T(\Delta r)$, we construct the probability distribution with a bin width δ, assume that the pairs of arbitrary fluorophores ($pairs(i)$) within each distance bin i is large, and use the distances between localizations that are separated in time by N. The approximate true probability of observing a distance within bin i is then the following:

$$P_d^i(\Delta r|\Delta n = N) = \frac{\sum_{w=1}^{pairs(i)} \phi}{\sum_{q=1}^{All_{pairs}} \phi} \approx \frac{pairs(i) \times \overline{\phi}}{All_{pairs} \times \overline{\phi}} = \frac{pairs(i)}{All_{pairs}} = P_T^i(\Delta r), \quad (1)$$

where All_{pairs} is the number of pairs of fluorophores, $\overline{\phi}$ is the mean of the random variable and $P_d^i(\Delta r|\Delta n = N)$ is the bin i of the pairwise distance distribution between all localizations separated by the given frame. Equation 1 shows that with the previously mentioned assumptions the probability of finding a distance within each bin will be identical to that of the true pairwise distance distribution, justifying the principle. Note that each frame difference larger than N can be used to approximate the true pairwise distance distribution, therefore creating the pairwise distance distribution using all distances between localizations that are separated by a frame difference larger than N leads to an even better approximation of the true pairwise distance distribution.

3 Error From Small N

We have shown that depending upon the experimental system and imaging conditions, the photobleaching lifetime of a fluorophore can greatly vary. If the total number of frames used in SMLM imaging is not large enough, *i.e.* a significant portion of fluorophores does not photobleach throughout the acquisition, it can lead to errors in determining the true pairwise distance distribution. Using simulations, we show that

the percentage of over-counting approaches the percentage of fluorophores not bleached after N frames. Therefore, one should select fluorophores that can photobleach relatively fast compared to the imaging timescale to use with DDC. When in doubt, one should use larger values of N, longer imaging times, and use the normalized Z score $v.s.$ Δn plot as that shown in main text Fig. 1D to determine a minimal N value (again larger N values should be utilized when in doubt).

To illustrate this principle, we simulated a fluorophore (Fig. S3A) that bleaches over a timescale of approximately 2000 frames (Fig. S3B). We then quantified the degree of over-counting based on the true pairwise distance distribution when different N values were used. To do so, we calculated the apparent "true" pairwise distance distribution of the same imaging sequence but stopped at different N values, and used this apparent "true" distribution to apply DDC to eliminate repeat localizations. We then divided the total number of "true" localizations determined from this exercise by the true number of the fluorophore used in the simulation, obtaining the average number of localizations per fluorophore l at different N values. The overcounting error percentage e is calculated as $e = (l - 1) \times 100$
.
In Fig. S3C, at lines corresponding to different N values, we show the proportion of fluorophores bleached and the average number of localizations per fluorophore at that N value. As expected, the degree of over-counting decreases with increasing N and roughly corresponds to the percentage of fluorophores not bleached at N frame. For example, at $N = 420$, 17% = 1 - 83% of fluorophores remained unbleached, and the average number of localizations per fluorophore is 1.2, corresponding to an overcounting error of 20%.

4 The Inner Workings of DDC

We first present all of the technical details and derivations for the application of DDC. Second, we present a simple toy model to illustrate how the different parts of DDC work together to correct for blinking artifacts.

4.1 Defining the Likelihood

Here we define the Likelihood as the following:

$$\mathcal{L}(\{R,T\}|\mathbf{r},\mathbf{n}) = \prod_{i,j\in\{T\}} P_T(\Delta r_{i,j}) \times \prod_{i\in\{R\},j\in\{R,T\}} P_{R1}(\Delta r_{i,j}|\Delta n_{i,j}), \tag{2}$$

where $\{R,T\}$ are sets that contain the indices of the localizations that are considered the repeats $\{R\}$ and the true localizations $\{T\}$, where both sets account for every localization. The actual experimental data are stored within the two terms $\mathbf{r}$ & $\mathbf{n}$, with the prior containing the coordinates of every localization and the later containing the frame. The first term on the right determines the probability of observing all of the distances between every pair of true localizations. Here the probability distribution $P_T(\Delta r_{i,j})$ is the true pairwise distance distribution, which gives the probability of observing a distance Δr between the two localizations i & j if they are both true localizations. The second term is the probability of observing all of the distances between the pairs of localizations if at least one is considered a repeat. Here, the probability distribution $P_{R1}(\Delta r_{i,j}|\Delta n_{i,j})$ gives the probability of observing the distance between the pair of localizations given the frame difference between them if at least one of the localizations is a repeat. Note that every pair of localizations are within the likelihood calculation no matter which localizations are assigned to the sets $\{R$ & $T\}$.

Overall, by maximizing the Likelihood a subset of true localizations is determined, where the pairwise distances between the true localizations are independent of frame, Δn, and follow $P_T(\Delta r)$. Below we

provide all additional information needed to calculate $\mathcal{L}(\{R,T\}|\mathbf{r},\mathbf{n})$. First we discuss how to determine the second distribution $P_{R1}(\Delta r_{i,j}|\Delta n_{i,j})$ and second the methodology for determining the two sets $\{R\ \&\ T\}$.

4.1.1 Determining $P_{R1}(\Delta r|\Delta n)$

To determine $P_{R1}(\Delta r|\Delta n)$ we utilize the pairwise distance distributions between localizations with a given frame $P_d(\Delta r|\Delta n)$ and the true pairwise distance distribution $P_T(\Delta r)$. Here $P_T(\Delta r)$ is known, determined using the pairwise distances between localizations that are separated by a frame greater than N (See Main Text).

Again, the desired distribution $P_{R1}(\Delta r|\Delta n)$ gives the probability of observing a distance between localizations for a given Δn if at least one of them is a repeat. $P_{R1}(\Delta r|\Delta n)$ is therefore made up of the distances between $\{R$ and $T\}$ and $\{R$ and $R\}$, where the curly brackets with the *and* indicate the pairwise distances between the localiztions within the sets. While $P_d(\Delta r|\Delta n)$ is made up of the distances between $\{R$ and $T\}$, $\{R$ and $R\}$, and $\{T$ and $T\}$ for a given Δn. Therefore, $P_{R1}(\Delta r|\Delta n)$ is equal to $P_d(\Delta r|\Delta n)$ with the contribution from the distances between true localizations removed, $\{T$ and $T\}$.

To properly eliminate the part of the distribution that is due to the distances between the true localizations, we quantify the makeup of $P_d(\Delta r|\Delta n)$ and then proportionally remove $P_T(\Delta r)$ from $P_d(\Delta r|\Delta n)$, resulting in $P_{R1}(\Delta r|\Delta n)$.

$P_d(\Delta r|\Delta n)$ is itself a combination of two distributions $P_T(\Delta r)$ & $P_{blink}(\Delta r)$, where the distances between different fluorophores follow $P_T(\Delta r)$ [Categories C1 and C2] and the distances between localizations from the same fluorophore follow $P_{blink}(\Delta r)$ [Category C3]. Here the probability distribution $P_{blink}(\Delta r)$ is the probability of observing a distance between a pair of localizations that are from the same fluorophore [Category C3] and is determined by the resolution of the SMLM experiment.

We can determine $P_{blink}(\Delta r)$ by comparing $P_T(\Delta r)$ to $P_d(\Delta r|\Delta n < N)$. The distribution $P_T(\Delta r)$ by definition lacks all distances between pairs of localizations that are from the same fluorophore and only contains distances between localizations from different fluorophores [Categories C1 and C2]. While $P_d(\Delta r|\Delta n < N)$ not only contains the distances between pairs of localizations from the same fluorophore [Category C3], but the distances between different fluorophores [Categories C1 and C2]. Note that within a SMLM experiment the resolution is very high, and therefore the distances between the localizations from the same fluorophore are very small, much less than 1000 nm. Therefore, the "shape" of the tails of the two distributions $P_T(\Delta r)$ and $P_d(\Delta r|\Delta n < N)$ match each other, as they both only contain the distances between different fluorophores (Data not shown). With this understanding in mind, the distribution $P_{blink}(\Delta r)$ can be obtained by subtracting $P_T(\Delta r)$ from $P_d(\Delta r|\Delta n < N)$ so that the probability of observing a distance greater than 1000 nm is approximately zero, and then normalizing so that the distribution sums to one.

To determine the proportion of each distribution making up $P_d(\Delta r|\Delta n)$, $P_d(\Delta r|\Delta n)$ can be fit to the following equation:

$$X(\Delta n) = Fit[(1-X)\times P_{blink}(\Delta r) + X \times P_T(\Delta r)], \tag{3}$$

where X is between 0 and 1.

The proportion of the distances that follow $P_T(\Delta r)$ come from the distances between $\{T$ and $T\}$ and $\{R$ and $T\}$. We must therefore take this into consideration when determining the proportion of $P_{R1}(\Delta r|\Delta n)$ that follows $P_T(\Delta r)$. To adjust the proportion of the distribution that follows $P_T(\Delta r)$ we calculate the ratio of the number of distances from $\{R$ and $T\}$ relative to the number of distances from $\{T$ and $T\}$ and

$\{R \text{ and } T\}$.

This ratio can be determined by calculating the average number of repeats per fluorophore, num_b. num_b can be obtained without having to perform any additional experiments, using the approximate probability that a localization is a repeat (See Approximating the Probability a Localization is a repeat Section of this Supporting Material) and Alg. 1 to obtain a relatively accurate estimation as to the number of blinks per fluorophore. (Note: for this calculation $\kappa(density) = 0$ and $\kappa_2(frame) = 0$, discussed later.) Here we should note that num_b could also be determined by experiment, though these experiments can be difficult and are very sensitive to model specific errors.

The ratio of the number of distances from $\{R \text{ and } T\}$ relative to the number of distances from $\{R \text{ and } T\}$ and $\{T \text{ and } T\}$ is then the following (See Mathematical Justification Section of this Supporting Material):

$$\alpha = \frac{num_b + num_b + num_b * num_b}{1 + num_b + num_b + num_b * num_b} = \frac{\#\{R \text{ and } T\}}{\#\{R \text{ and } T\} + \#\{T \text{ and } T\}}. \tag{4}$$

where $\#\{R \text{ and } T\}$ indicates the number of distances between the localizations within the two sets. The distribution $P_{R1}(\Delta r|\Delta n)$ is then equal to the following equation:

$$P_{R1}(\Delta r|\Delta n) = Norm[P_T(\Delta r) \times X(\Delta n) \times \alpha + P_{blink}(\Delta r) \times [1 - X(\Delta n)]]. \tag{5}$$

Here $Norm$ indicates that the distribution within the brackets is normalized so that it sums to one. The distribution $P_{R1}(\Delta r|\Delta n)$ is a combination of the two distributions that are from the distances between localizations from different fluorophores ($P_T(\Delta r)$)) and the distances between the localizations from the same fluorophore ($P_{blink}(\Delta r)$). The first term ($P_T(\Delta r) \times X(\Delta n) \times \alpha$), first accounts for the proportion of the distribution $P_d(\Delta r|\Delta n)$ that results from the distances between localizations from different fluorophores and then scales this proportion further with α, so that the contribution from the distances between the pairs of true localizations are removed. $P_{R1}(\Delta r|\Delta n)$, for the 1 dark state no clustered simulation is shown in Fig. S6A. As expected, there is a large probability for small distances and small frame differences due to the proportion of distances between the blinks of the same fluorophores being large. Then as the frame difference increases, the proportion of distances between the blinks of the same fluorophores decreases and the distribution converges upon the true pairwise distance distribution, Fig. S6A.

4.1.2 Determining the sets {R} and {T}

To assign a localization to either the {R} set (repeat) or the {T} set (True Localization) DDC uses the following:

$$\{R, T\} = Alg_1[\mathbf{r}, \mathbf{n}, \mathbf{M}, \kappa(density), \kappa_2(frame)]. \tag{6}$$

The sets {R} and {T} are determined within *Algorithm* 1, which uses the parameters and data within the brackets to assign each localization to one of the two sets. The actual experimental data are stored within the two terms **r** & **n**, where **r** contains the coordinates of each localization and **n** contains the frame. Here, **M** is a matrix that contains the information that is used to determine the probability that a localization is a repeat (See Approximating the Probability a Localization is a repeat Section) and $\kappa(density)$ & $\kappa_2(frame)$ are monotonic functions that are determined within the MCMC. The two functions $\kappa(density)$ & $\kappa_2(frame)$ allow DDC to adjust the probability calculation by taking into consideration the local density of the image and the frame of each localization. These are the two functions that vary during the MCMC to maximize the likelihood, defining the two sets. We discuss the specifics of $\kappa(density)$ & $\kappa_2(frame)$ within the section Alg. 1, Linking Localizations into Trajectories.

4.2 Approximating the probability that a localization is a repeat

Depending upon the number of localizations within a SMLM image, the number of subsets of localizations can be extremely large. To speed up the phase space search and to minimize the likelihood of overfitting DDC calculates the approximate probability that each localization is a repeat (within the blinking trajectory) of a prior localization and only investigates the more likely subsets of localizations using the MCMC approach (Alg. 1, Linking Localizations into Trajectories). Below we discuss how the approximate probability that each localization is a repeat can be determined and then describe Algorithm 1, which defines which localizations are true localizations and which are repeats within DDC.

Here we define the matrix $\mathbf{M}$, which gives the probability that a localization is a repeat of a prior localization given a distance, Δr, and Δn between the localizations.

$$\mathbf{M}(\Delta r \in i, \Delta n) = \frac{P_d^i(\Delta r|\Delta n) - \omega \times P_T^i(\Delta r)}{P_d^i(\Delta r|\Delta n)}, \tag{7}$$

where $P_d^i(\Delta r|\Delta n)$ is the raw probability for the distance between two localizations to be in bin i, given that they are separated by Δn, $P_T^i(\Delta r)$ is the true pairwise distance distribution and $\omega = \frac{\sum_{i>>\sigma} P_d^i(\Delta r|\Delta n)}{\sum_{i>>\sigma} P_T^i(\Delta r)}$, where σ is the localization precision of the microscope. Here ω is a scaling factor used to match the tails of the two distributions, as the distance distributions have a similar shape for $\Delta r >> \sigma$. Fig. S5 illustrates this calculation and the assumption about the tails of the distribution. $\mathbf{M}$, for the 1 dark state no clustered simulation is shown in Fig. S6B, as expected, there are high probabilities with small Δr and small Δn, which get lower as Δr and Δn increase. $\mathbf{M}$ is the matrix that Alg. 1 uses to link localizations into trajectories.

4.3 Alg. 1, linking localizations into trajectories

Here we describe Alg. 1, which DDC uses to determine which localizations are linked into trajectories using the previously defined $\mathbf{M}$ and $\kappa(density)$ & $\kappa_2(frame)$. (See Approximating the Probability a Localization is a repeat) Note: one could easily modify the algorithm and have it take into consideration more information to determine which localizations belong to each set, but at a computational cost and risk of overfitting.

We wanted our methodology to be able to account for heterogeneous distributions of fluorophores within the same image and to incorporate the "time" dependence for the appearance of localizations. Therefore, one single cutoff probability or threshold was avoided. Instead we made the probability at which localizations are linked together into the same blinking trajectory related to the local density of the image before blinking correction and related to the frame of the localization.

Note: during the maximization of the likelihood for all of the systems within this work, we could not simply eliminate localizations without taking into consideration the "probability of repeat", as this led to an extremely large phase space and did not converge within a reasonable amount of time.

Here the reasoning for incorporating the density is this: the more dense a region of an image is the more likely that a true localization could be considered a repeat by chance (based off of the probability calculation, see Alg. 1) and therefore the density of the image needs be taken into consideration. To incorporate the heterogeneity of the image DDC determines the local density of each localization before the blinking correction. To do this DDC calculates the number of raw localizations that are within 2σ (SMLM resolution) and have a frame difference greater than N, for each localization. DDC then defines a monotonically increasing function that is a function of the density, $\kappa(density)$ [Initially $\kappa(density) = 0$]. The flexibility of this function allows DDC to handle heterogeneous distributions of fluorophores by taking

into consideration the local density of the image for the probability calculation (See Alg. 1).

Note: the shape of this function is determined during the MCMC approach and is discussed within Alg. 2.

The reasoning to include the frame information within the probability calculation is: because more localizations appear at the beginning of the acquisition of an image when compared to the end of the acquisition, localizations would be more likely to be considered repeats at the beginning of the acquisition than at the end by random chance. (Because fluorophores photo-bleach during the acquisition of a SMLM image.) The time dependence is utilized in a similar manner as the density, where a monotonically decreasing function of the frame of each localization is incorporated into the probability calculation, $\kappa_2(frame)$, see Alg 1.

Note: the shape of this function is also determined during the MCMC approach and is discussed within Alg. 2.

To link localizations into trajectories DDC utilizes Alg. 1. This simple algorithm goes through all localizations and links them into trajectories, starting with the localizations that are most similar in frame. To decide whether or not to link two localizations into the same trajectory [or two trajectories into one] the algorithm used the mean of the "probabilities of blink" of the localizations being considered. DDC calculates the probability of being a blink with the matrix $\mathbf{M}$, and then divides the mean probability by $1+\kappa(density(ii))+\kappa_2(frame(ii))$. This takes into account the local density and frame of the localization ii. If the probability of the localization [or localizations] is larger than .5, then the localizations are combined into the same trajectory. For each trajectory all localizations but the localization with the smallest frame in each trajectory are then considered repeats.

Note: we should mention that the order in which the localizations in Alg. 1 are arranged does have a small influence on the trajectories that are formed, especially if the activation rate is high. Therefore, DDC also varies the order of the localizations during the MCMC approach to obtain different subsets of true localizations (See Alg. 2 of this Supporting Material for further details.)

Note: we found that not including an algorithm of similar structure to Alg. 1 (takes into account the physical process of fluorophore blinking) either resulted in an extremely slow convergence or got stuck in minimums that deviated from the true image. Therefore, including the information within $\mathbf{M}$ is critical for DDC to converge upon the true image. We should also state that we did not perform an extensive search for alternatives and we do realize that improvements to Alg. 1 could be an area of improvement for DDC in future research.

4.4 Alg. 2, MCMC approach to maximize the likelihood

Here we describe Alg. 2, which DDC uses to maximize the Likelihood and obtain the "correct" subset of true localizations.

Algorithm 2 is a simple Markov Chain Monte Carlo (MCMC) approach that utilizes Alg. 1 in the process. The MCMC approach perturbs three parameters, $\kappa(density)$, $\kappa_2(frame)$ and the order of the localizations to determine the "correct" subset of true localizations. For each step, one of the three previous parameters are modified by a small amount and the likelihood is calculated for the particular subset of true localizations determined by Alg. 1, given those parameters. Alg. 2 then keeps the new parameter and resets the best likelihood if the likelihood is greater than the previous best likelihood or accepts the new parameters if the difference of the likelihood with the old likelihood is greater than a log of an uniform random number. An example of a phase space search is shown in Fig. S7, where the maximization of the likelihood results

in the results shown in red.

We found that including the MCMC approach to maximize the log of the likelihood led to significant improvements in the correct number of fluorophores calculated for all systems. Furthermore, for the more heterogeneous distributions of localizations, the Small clusters simulation systems, the MCMC approach led to dramatic improvements in the image error, data not shown. Therefore, the MCMC approach is vital to the successful supplication of DDC even though it is the most computationally expensive step of the methodology.

4.5 Toy model illustration for Alg. 1 and Alg. 2

In Extended Data Figure 4A we show a simple toy model system that illustrates a simplified understanding of the inner workings of DDC. This example has 6 localizations total (4 true localizations (black) and 2 repeat localizations (purple)). The frame of each localization is the closest colored number in Extended Data Figure 4A. For this specific example the distance between a pair of localizations is either "small" or "large".

By using the above derivations one can easily obtain the true pairwise distance distribution and the distribution of observing a distance between a pair of localizations given at least one is a repeat for a particular frame difference (Δn), Extended Data Figure 4B. Here we should emphasize that these are the distributions that provide the "ground truth" about the true underlying configuration of molecules — that is, when assigning localizations to be either a repeat or a true localization, the distances between the true localizations should follow P_T and the distances between localizations where at least one is a repeat should follow P_{R1}.

Note, for this particular example we have purposely only included repeats that appear upon the adjacent frame of their true localization — that way we only have one distribution for P_{R1} (in the "real world" there will be an additional distribution for each Δn up to N, creating many more constraints for the phase space search). Additional note, for this example one cannot determine the true pairwise distance distribution by using the distances between localizations separated by a frame difference greater than N because one needs a sufficient number of localizations for SI Equation 1 to hold.

In Extended Data Figure 4B we show the probabilities in parenthesis for observing either the small distance or the large distance and the individual pairs which contribute these distances for each distribution (P_T and P_{R1}); for example, the small distances of P_T are due to the distances between the localizations 10 to 4 and 1 to 3 (localizations identified by their particular frame). The likelihood equation is shown below, with the number of distances in each bar for the distributions assigned to the variables "a" through "d" — this illustrates what one is trying to obtain when maximizing Lik.

With this understanding of the likelihood, in Extended Data Figure 4C we show how algorithms 1 and 2 work together to eliminate the repeat localizations (aka. how they assign the sets and pick the best sets). Note, here we have simplified how Alg. 1 works while preserving the main idea behind the algorithm, see Alg. 1 for exact details on how it links localizations into trajectories.

Utilizing the matrix M (See above), Alg. 1 essentially computes the probability of whether a localization is a repeat. In the first step of the MCMC (Alg. 2) there is no bias introduced, and the raw calculated probability matches the varied probability. This is illustrated in Extended Data Figure 4C as the black bars (raw calculation) and green bars (varied) for each localization. If the probability of being a repeat (green bar) is greater than .5, then the localization is considered a repeat, resulting in new sets. In Extended Data Figure 4D, we show how the sets in (C) change the distances within the different parts of the

distributions creating a new Lik, the goal of DDC is to find the sets which maximize Lik.

To do this, Alg. 2 then perturbs/varies the calculation by a small amount resulting in new green bars and new sets. This results in a Lik (due to the new values of [a, b, c, and d]), if the Lik is larger (or within error defined by the MCMC) the perturbation is accepted. Alg. 2 then continues creating new small perturbations to the previous steps green bars for a certain number of steps. The sets that result in the maximal likelihood are then output by DDC for the blinking corrected image.

5 DDC and Live Cell Superresolution Imaging

As with any other methodology that deals with blinking, live-cell imaging could make interpretations of images more complicated. Complications arise if fluorophores are able to "diffuse away" before they are bleached. If a molecule diffuses away before being actually bleached, DDC will still work, but will treat the molecule diffusing away as a bleaching step. Therefore, if the molecule shows up in a different location, DDC will count this as a new molecule, making counting difficult. Additionally, if there is "small scale" diffusion between frames, DDC will simply assign a lower resolution, and link molecules into trajectories that are farther away. Note: we did not investigate how more complicated models of diffusion would perturb DDC's performance or if different modes of diffusion exist.

6 Evaluating the three most common threshold methodologies and the absolute best image error from thresholding

Here we investigate the three most common threshold methodologies and compare their results with DDC. We also compare DDC to the absolute best Image Error thresholding can produce. We discuss the results from each of the comparisons here and whenever we reference the 2 dark state systems we are referring to Fig. 2 in the main text and whenever we mention the 1 dark state system we are referencing the results shown in Fig. S10.

6.1 Equations for evaluating the different methods

The image error of each methodology was calculated with the following equation:

$$ImageError = \frac{\sum_{i,j}[Norm(CorrectedImage(i,j)) - Norm(RealImage(i,j))]^2}{\sum_{i,j}[Norm(UncorrectedImage(i,j)) - Norm(RealImage(i,j))]^2}, \tag{8}$$

where $i\&j$ go over all pixels within the images, Norm() indicates that the image is normalized so that the maximum intensity is 1 and the lowest intensity is 0, CorrectedImage is the image that results from a blinking corrected methodology, RealImage is the image that results if an image is generated only using the true localizations and UncorrectedImage is the image with no blinking corrected methodology.
The counting error of each methodology was calculated with the following equation:

$$CountingError = \frac{|Methods\#ofloc - Real\#ofloc|}{Real\#ofloc} \times 100, \tag{9}$$

where $Methods\#ofloc$ is the number of true localizations determined by the methodology and $Real\#ofloc$ is the actual number of true localizations.

6.2 Specific details about T1

Our T1 is similar to that within Betzig et al. (1), this (first) thresholding methodology approximates the photo-kinetics of the fluorophore from the actual data itself, which is then used to approximately correct for blinking by setting a time threshold "encompassing" the off times of the molecules. The photo-kinetics of fluorophores are often approximated utilizing a semi-empirical formula developed in 2011 (2). Here the main benefit is that one does not need to do additional experiments to quantify the photo-kinetics of the fluorophore. Additionally, within Annibale et al. they stated that one can obtain images free from cluster artifacts by choosing a significant time threshold, "moving into the missed counts regime" — which for their methodology was approximately equal to using a time threshold 2 times the average dark time of the fluorophore (or greater than 2 times the average off time) (1). Coltharp et al. (3) also found ("roughly") that the optimal time threshold was equal to approximately 2 times the average dark time of the fluorophore, and a time threshold equal to two times the longest average dark time has been used before (4, 5). Therefore, we set the time threshold of the T1 methodology equal to 2 times the average off time. Note, if a system had multiple off states we set the time threshold equal to 2 times the longer off state.

For the Annibale et al. methodology the distance threshold is set to 1 pixel (100nm) and the time threshold, t_d (dark time) is varied and the number of localizations at each t_d is quantified and fit with an empirical equation. To evaluate the effectiveness of this methodology we applied the methodology to the 1 dark state simulation data for the three different distributions of fluorophores, Fig S8. The error in the number of fluorophores and the average dark time was significant (The percent error for the extracted parameters is shown in the titles of each subplot.)

Considering the error in the extracted parameters for the simulation systems, Fig. S8, we chose to assume that the T1 methodology had perfect knowledge of the timescales for the dark states for each simulation system. We set the T1 distance threshold to 2 times the resolution and set the time threshold equal to 2 times the average dark time. For the two dark state simulation data we set the time threshold equal to 2 times the longer dark time. The results of applying these thresholds are shown in Fig. 2 in the main text. When we applied the T1 methodology on real experimental data, we utilized the values from the fits to determine the time thresholds — that is, 2 times the longer off time for the time threshold.

6.3 Specific details about T2

For the thresholding methodology of Puchner et al. (6), they first characterized the photo-kinetics of the fluorophore and then set an extremely stringent time threshold, so that 99% of blinking dark times would be linked together and a distance threshold equal to 4 times the resolution of the experiment. This methodology was mainly developed to eliminate the possibility of blinking leading to the appearance of clusters, but due to the extreme thresholds this method will deplete the intensity of true clusters.

The results of comparing this thresholding methodology to the 1 dark state simulation systems is shown in Fig. S10. For the Image Error in each of the 3 systems DDC was significantly better than this thresholding methodology. The improvement was especially noticeable for the dense 1 dark state system, as the stringent thresholds are expected to be detrimental to dense clusters. Suggesting that DDC is better at obtaining the true underlying distribution of fluorophores.

Interestingly, this methodology performed especially well for the number of fluorophores in the random and Small clusters 1 dark state systems, but failed for the dense system with a percent error around 15%. When compared to DDC for the number of fluorophores, DDC consistently had a percent error less than 5%. Suggesting that DDC is also a more reliable method under this metric for this fluorophore.

The results for comparing this thresholding methodology with DDC for the 2 dark state simulation systems is shown in Fig. 2 in the main text. Across the board DDC was vastly better than this thresholding methodology for both the Image Error and the error in the number of fluorophores. Suggesting that when the photo-kinetics of the fluorophore are more complicated than a simple 1 dark state DDC is especially beneficial when compared to this methodology. Furthermore, this thresholding methodology requires the characterization of the fluorophore, which wastes valuable time and can be experimentally difficult at times.

6.4 Specific details about T3

In the methodology developed by Coltharp et al. (3) they characterized the fluorophores to determine the number of blinks per fluorophore to determine the time threshold and the distance threshold. To determine the number of blinks per fluorophore Coltharp et al. utilized a low activation (UV) laser and slowly activated the fluorophores so that individual time traces could be easily extracted. In the last section of the results of the main text we show that this methodology is likely flawed and varying activation intensities change the photo-physics of the fluorophores potentially leading to errors in the number of blinks per fluorophore, Fig. 4. Though, further experiments would be needed for that particular fluorophore. Also, even if the time traces are properly extracted from fluorophores with the same photo-physics the fits to the dark time intervals are error prone and model dependent (3).

Assuming perfect knowledge as to the number of blinks per fluorophore for this methodology, we scanned the number of localizations obtained for each time threshold and distance threshold. The ideal thresholds were determined using the thresholds for the minimal error in the number of localizations at the intersection of the time and distance thresholds. Examples of this phase space search for six different systems investigated in this work are shown in the first column of Fig. S9, with the corresponding Image Error for each set of thresholds shown in the second column. (Note: the error is log scale for the first column so one can clearly see why the exact thresholds were chosen.) The thresholds determined by this methodology are shown in the following table:

System	Time Threshold (n)	Distance Threshold (nm)
Random 1 dark	25	130
Small clusters 1 dark	20	130
Dense 1 dark	20	100
Random 2 dark	35	130
Small clusters 2 dark	35	130
Dense 2 dark	30	100
Filament	35	80
Continuous Filaments	34	60

Note: Logically, the optimal thresholds for this methodology became less intense the more dense the molecular distributions became.

The results of applying this methodology are shown in Fig. S10 for the 1 dark state systems and Fig. 2 for the 2 dark state systems. Considering with this methodology we assumed perfect knowledge for the number of blinks per fluorophore it was of little surprise that the error in the calculated number of fluorophores was actually lower than DDC for the 1 dark state systems. The error in the number of fluorophores was less than 6% for both methods for all systems for the 1 dark state fluorophore. Even though the error in the number of fluorophores for both methodologies was comparable, the DDC Image Error was lower for each 1 dark state system when compared to this thresholding methodology. Suggesting, that DDC captures a more reliable representation of the true localizations, while resulting in a comparable error in the number

of fluorophores for the simple 1 dark state fluorophore.

This was also the case for the 2 dark state simulation systems except for the dense distribution system. For the dense distribution system the error in the number of fluorophores was significantly worse for DDC, about 12%, while the thresholding methodology performed well with this metric. (We should note again that this is assuming perfect knowledge as to the number of blinks per fluorophore, so it is expected that the error in the number of fluorophores will always be low with this methodology.) Even though DDC performed worse for the dense 2 dark state system for the number of fluorophores, for the Image Error DDC greatly surpassed this thresholding methodology for all three distributions of fluorophores. The most significant improvement was for the dense system, where this thresholding methodology performed much worse than even an uncorrected SMLM image. Suggesting that DDC is vastly superior than this thresholding methodology for a more complicated 2 dark state fluorophore and great care should be taken when utilizing this methodology when actual clustering exists.

6.5 Specific details about T4

Considering DDC was able to surpass all of the traditional thresholding methodologies with regards to the Image Error, we wanted to see if any thresholds could surpass DDC. To do this we scanned the time threshold and distance threshold for each system and picked the thresholds that resulted in the mean minimum Image Error for each of the seven systems. The thresholds picked by this methodology are shown in the following table:

System	Time Threshold (n)	Distance Threshold (nm)
Random 1 dark	17	160
Small clusters 1 dark	13	170
Dense 1 dark	5	190
Random 2 dark	39	140
Small clusters 2 dark	28	150
Dense 2 dark	3	210
Filament	43	80
Continuous Filaments	10	80

The results of comparing the absolute best threshold methodology with DDC is shown in Fig. S10 for the 1 dark state system. As expected this thresholding methodology performed best for the metric of Image Error when compared to the other thresholding methodologies. Interestingly, DDC was still able to outperform the thresholding methodology in terms of the Image Error and in terms of the number of fluorophores.

The results of comparing this thresholding methodology with DDC for the 2 dark state system is shown in Fig. 2. Interestingly, for this fluorophore the Image Error and the error in the number of fluorophores for the Random and the Small clusters systems was similar between the two methods. The major difference was for the dense system where the error in the number of fluorophores was around 80% for the thresholding system, while DDC maintained an error of about 12%. Suggesting that the Image Error for the 2 dark state systems was similar between the two methods, but DDC was able to surpass this thresholding methodology in terms of determining the proper number of fluorophores.

These results suggest that even with the absolute best thresholds DDC is still a more reliable approach in regards to the two metrics investigated within this work.

7 Algorithms

Algorithm 1

procedure DETERMINE WHICH LOCALIZATIONS ARE BLINKS

$\mathbf{M}(\Delta r, \Delta n) \leftarrow$ Probability that a localization is a repeat of the preceding localization given the Distance and Frame between the preceding localization

$traj(i) \leftarrow$ is the trajectory that localization i is assigned (before the for loops each localization is assigned it's own personal trajectory)

$\Delta\mathbf{r}_{traj(i),traj(ii)}$ and $\Delta\mathbf{n}_{traj(i),traj(ii)} \leftarrow$ arrays containing the pairwise distances and frame differences between all localizations in the two trajectories containing localization(i) and localization(ii)

$\Gamma = length(\Delta\mathbf{r}_{traj(i),traj(ii)})$

$\kappa(density(i)) \leftarrow$ a monotonically increasing function that is dependent upon the local density of localization(i) without blinking correction (Supporting Material).

$\kappa_2(frame(i)) \leftarrow$ a monotonically decreasing function that is dependent upon the frame of localization(i) (Supporting Material).

{T}=1:length(Localizations) $\leftarrow$ the indices that are the true localizations

{R}=empty array $\leftarrow$ the indices of the localizations that are repeats

for Δn=1:max(frame) **do**

  for i=1:length(Localizations) **do**

    for ii={T} **do**

      if frame(ii)-frame(i)=Δn **then**

        if $\frac{[\sum_j^{\Gamma} M(\Delta\mathbf{r}_{traj(i),traj(ii)}(j),\Delta\mathbf{n}_{traj(i),traj(ii)}(j)]/\Gamma}{1+\kappa(density(ii)+\kappa_2(frame(ii))} > .5$ **then**

          Combine all the Localizations within the two trajectories into a single trajectory

          Eliminate Localization(ii) from {T} as it is now considered a repeat

          Include Localization(ii) in {R} as it is now considered a repeat

Algorithm 2

procedure MARKOV CHAIN MONTE CARLO TO MAXIMIZE LIKELIHOOD
    Max Lik=$-\infty$
    Count=1
    Number of Steps=1000
    while Count<Number of Steps **do**
        $\kappa(density(:)) = \kappa^{Stored}(density(:))$
        $\kappa_2(frame(:)) = \kappa_2^{Stored}(frame(:))$
        $C = rand \leftarrow$ a random uniform number
        if $C < 1/3$ **then**
            Adjust the function $\kappa(density(:))$ by a small amount
            Ensure that $\kappa(density(:))$ is still a monotonically increasing function of density
            Ensure that the mean of $\kappa(density(:))$ over all density values from all localizations equals zero
        else if $C < 2/3$ **then**
            Adjust the function $\kappa_2(frame(:))$ by a small amount
            Ensure that $\kappa_2(frame(:))$ is still a monotonically decreasing function of the frame
            Ensure that the mean of $\kappa_2(frame(:))$ over all localizations equals zero
        else
            Perturb the order of localizations that have the same frame ▷ This will change which localizations are linked together into the same trajectory
        $\{R, T\} \leftarrow$ Perform Alg. 1 with new $\kappa(density(:))$, new $\kappa_2(frame(:))$, and in new defined order
        Lik $\leftarrow$ Calculate log likelihood with new Corrected Localizations
        if Lik>Max Lik or $log(rand) < Lik - MaxLik$ **then**
            Store new parameters
            Max Lik=Lik
        else
            Go back to old parameters
        Count=Count+1

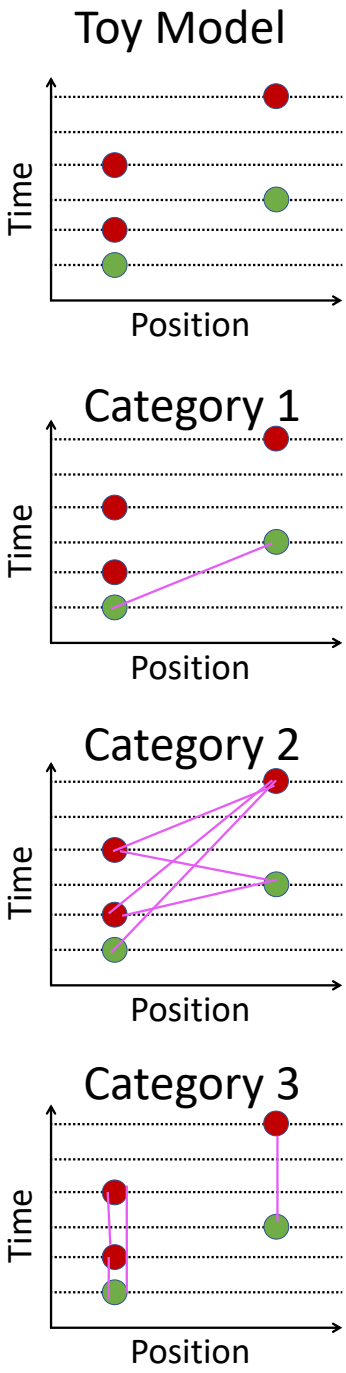

Figure S1: The top row shows a simple one dimensional system illustrating the blinking of two fluorophores, where the green dots are the true localizations and the red dots are repeats. The subsequent rows show the different categories referenced within the Supporting Material, with the pink lines illustrating the pairs of localizations for each category.

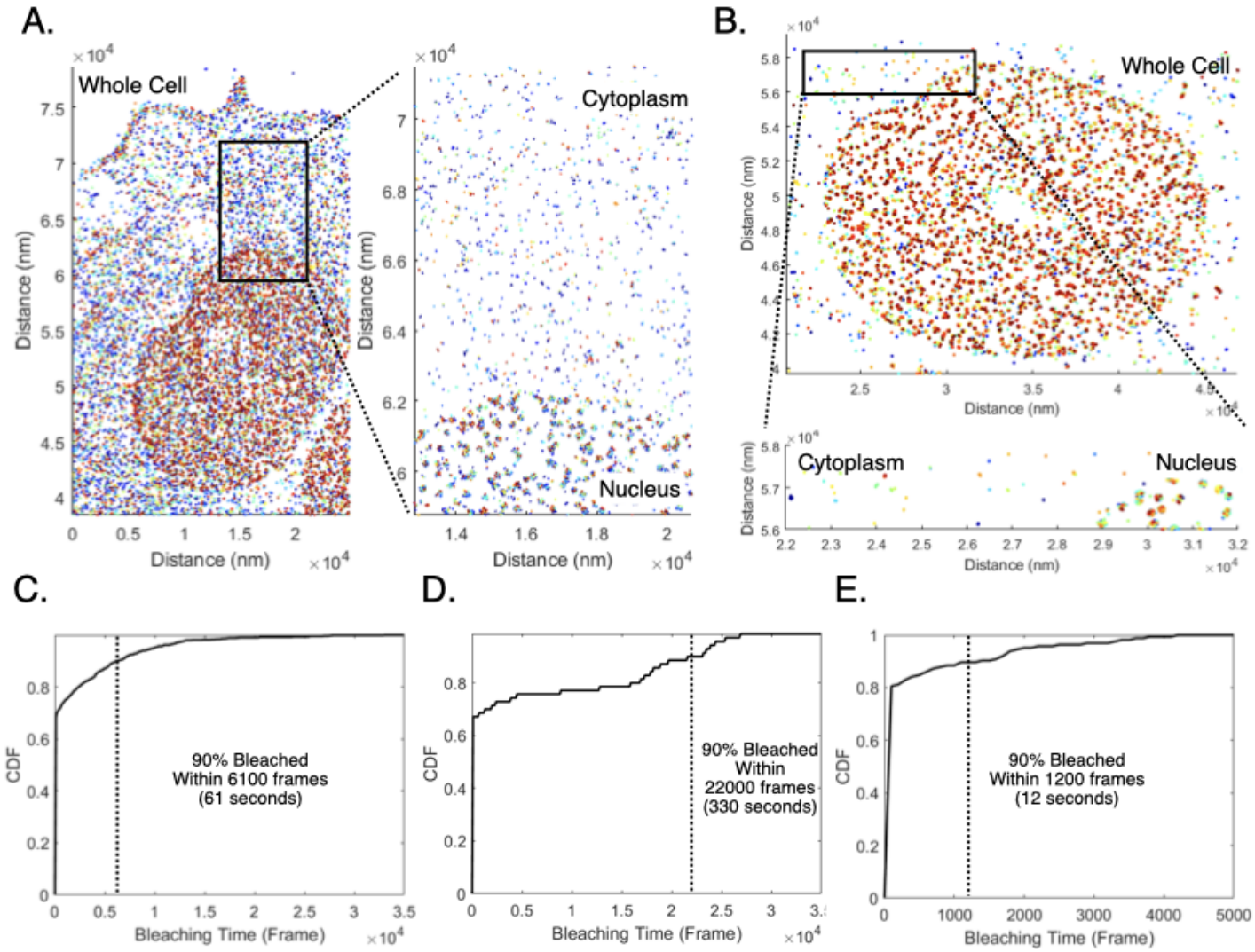

Figure S2: (A and B) Time-colored scatter plots of AF647-labeled nanobody molecules of the whole cell (left) and a zoomed-in section of the cytoplasm (right) in the NUP experiment performed in this study (A) and in Thevathasan *et al.* (7) (B). (C-E) Cumulative Distribution Functions of the photobleaching times of single AF647 fluorophores in the NUP experiment of this study (C), in Thevathasan et al. (D) and in the pre-rRNA experiment contributed to main text Figure 1D (E). The dashed line illustrates a timescale over which 90% of the fluorophores bleach.

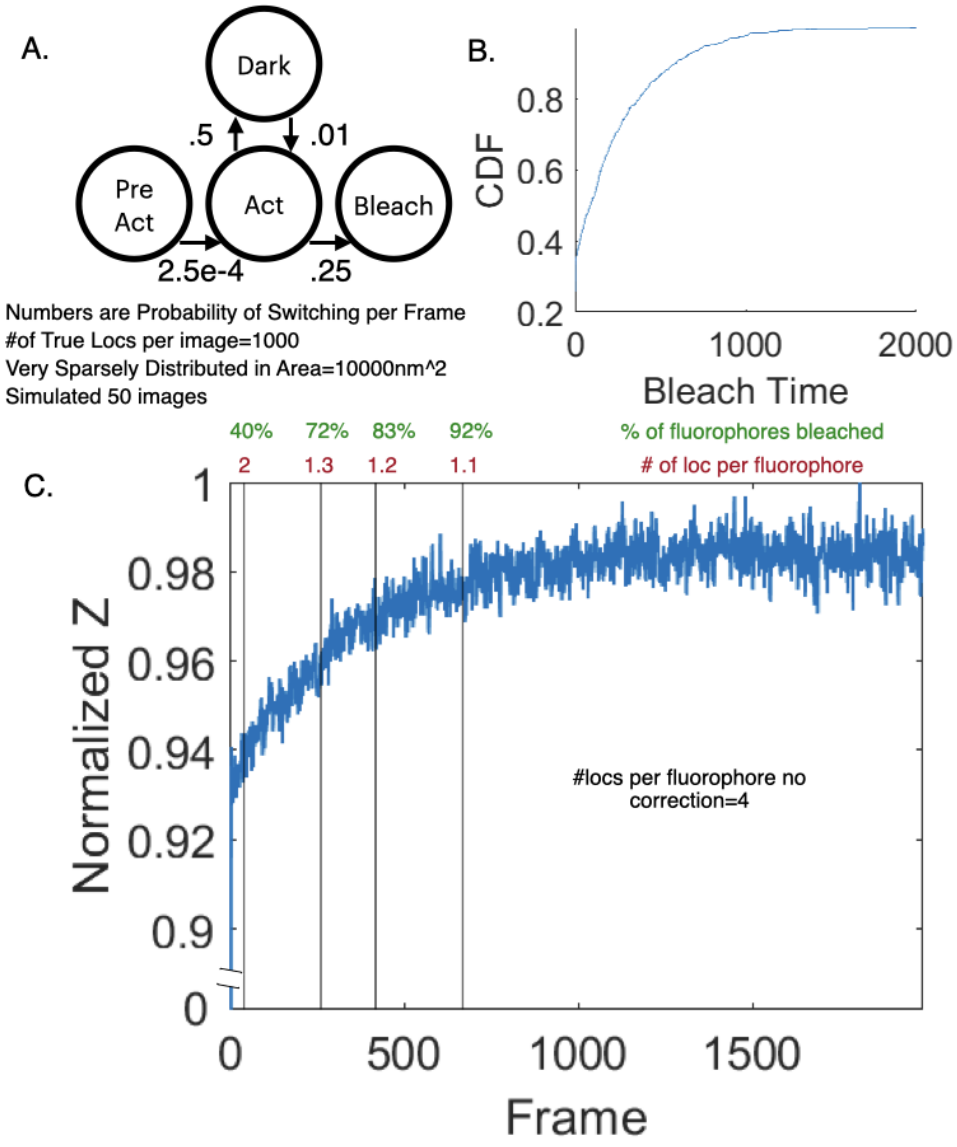

Figure S3: **Overcounting error reflects approximately the percentage of unbleached fluorophores at various N values.** (A) The photokinetic model of a fluorophore used in the simulation. (B) The Cumulative Distribution Function (CDF) of the bleach time of the fluorophore. (C) Normalized Z score $v.s.$ frame. Vertical lines indicate the various N values used to apply DDC to the imaging sequence. The green numbers are the percentage of molecules photobleached by frame N, and the red numbers are the average number of localizations per fluorophore determined at that N value.

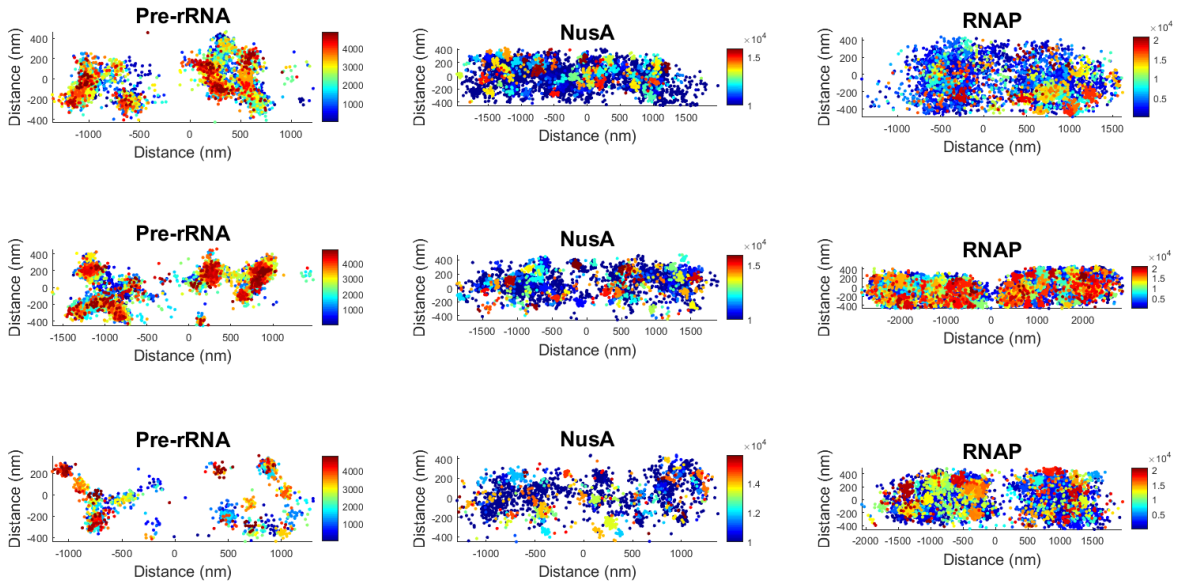

Figure S4: Example scatter plots of the experimental data used to verify that the pairwise distance distributions reached a steady state distribution. We show 3 cells for each molecular assembly, with the localizations colored with the frame of the localization.

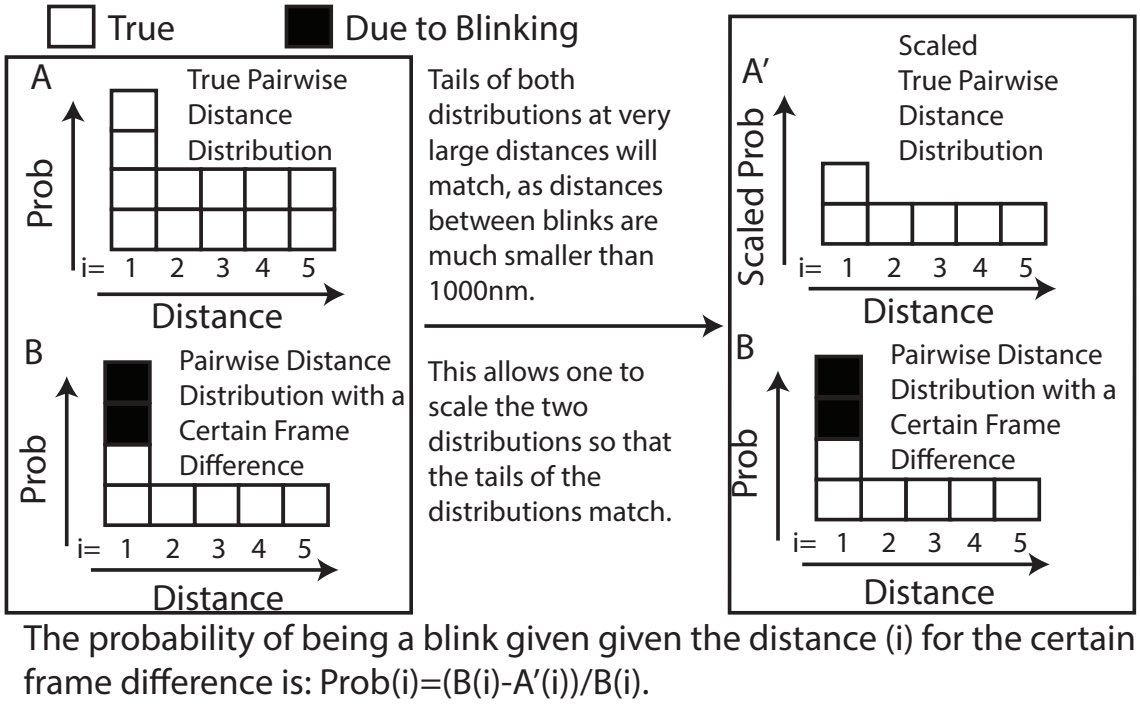

Figure S5: An illustration showing how to calculate $\mathbf{M}$ using the pairwise distance distributions. The blocks represent the distributions and i is the distance bin.

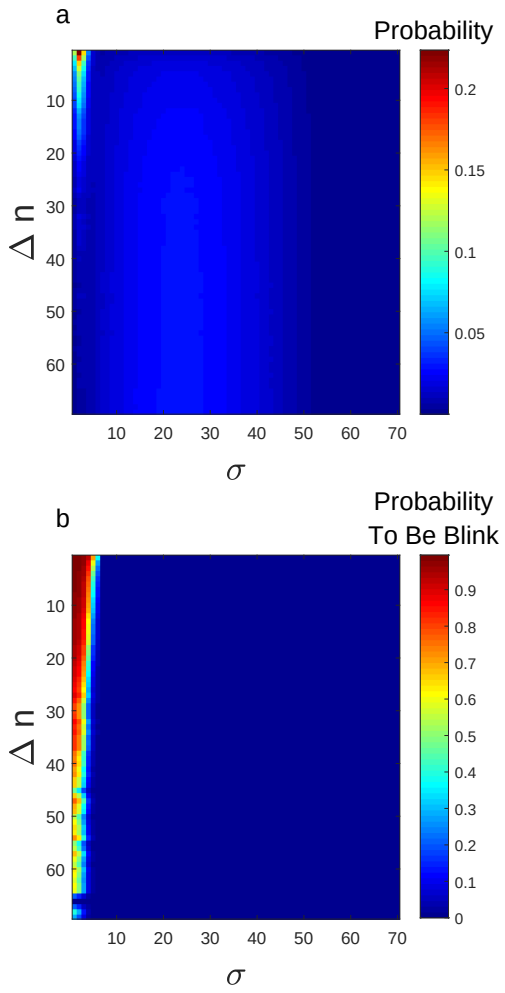

Figure S6: a. The probability distribution to observe a distance for a given Δn , in units of resolution σ, between two localizations when at least one of them is a repeat, $P_{R1}(\Delta r|\Delta n)$. This specific distribution is for the 1 dark state no clusters system. (See Supporting Material text for details as to how these distributions are used to calculate Likelihood) b. The probability that a localization is the repeat of a given localization given the frame and distance between the localizations. These probabilities are calculated using the calculation shown in the prior figure.

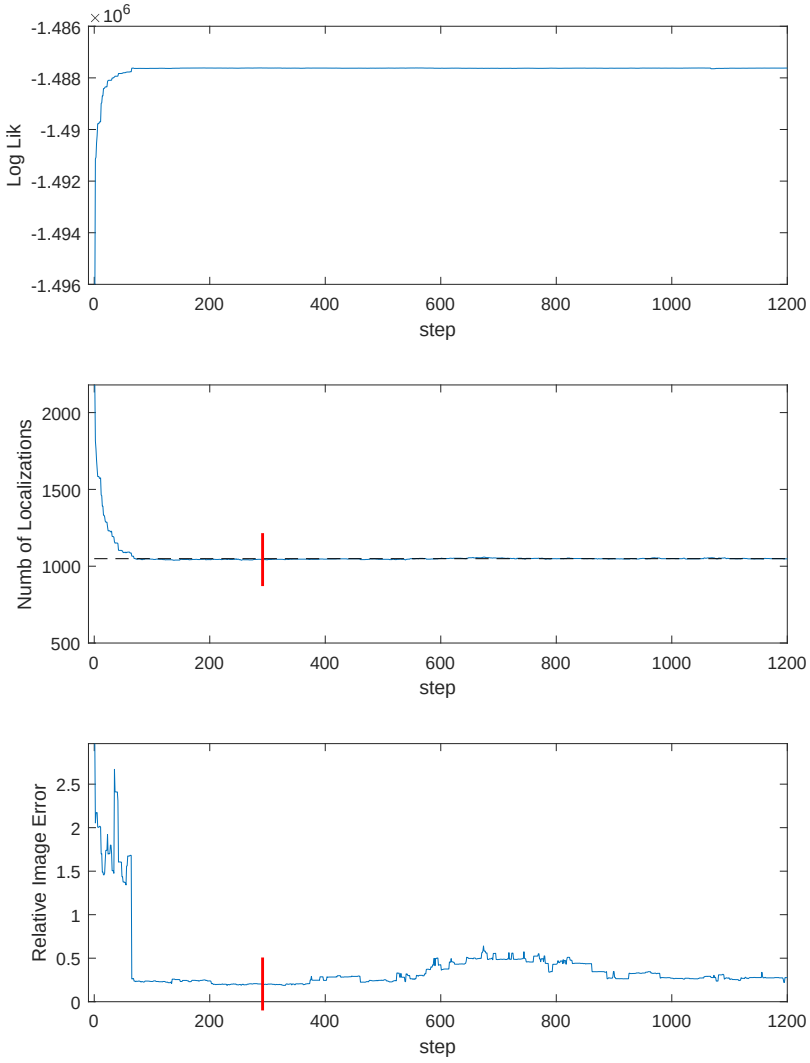

Figure S7: An example of the MCMC phase space search for the 2 dark state Small clusters system. For the number of localizations subplot a dashed black line shows the true number of localizations. For the bottom two subplots we show red lines indicating where the Likelihood was maximized. [Note: here we chose a random starting position for $\kappa(density)$ to illustrate the burn in phase of the MCMC, when $\kappa(density)$ starts at zero the burn in phase is not so extreme.]

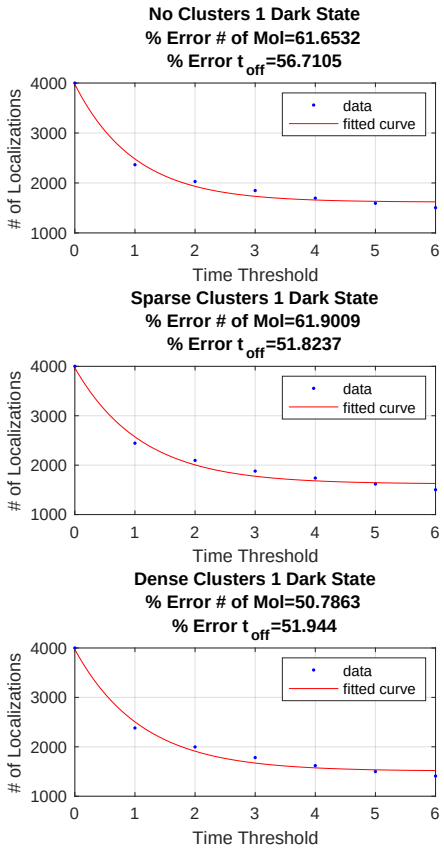

Figure S8: Resulting Error in Using Methodology of Annibale et al. (1): Here we only show the results for the 1 dark state systems with the fits to the semi-empirical formula (See Text). In the titles of each subplot we show the percent error in determining the number of true localizations and the average dark time.

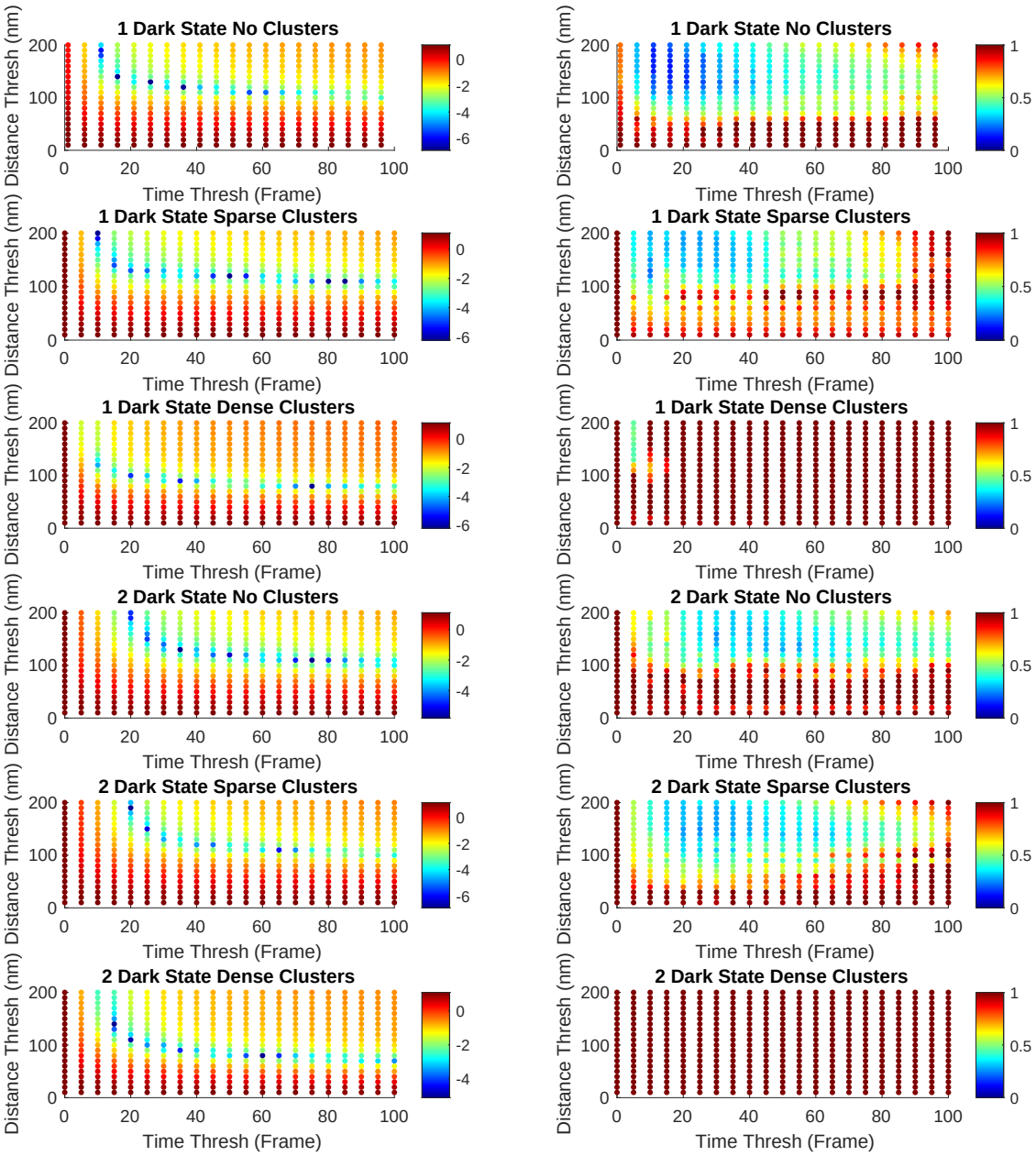

Figure S9: Determining the Thresholds for the Coltharp et al. Approach: In the first column we show the difference from the true number of localizations for the various time thresholds and distance thresholds, log scale ($ln[abs(\#loc - \#loc_{true})/\#loc_{true}]$. In the second column we plot the Image Error for each pair of threshold values for six systems.

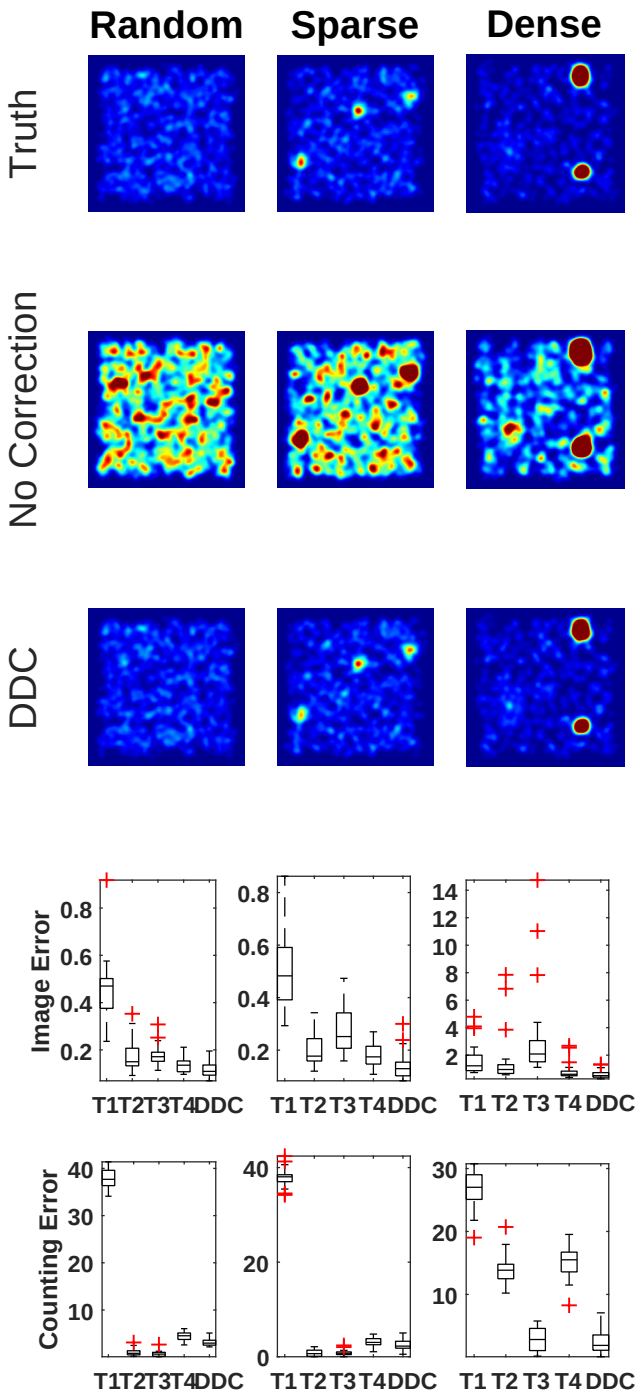

Figure S10: A comparison of the various thresholding methodologies with DDC and no blinking correction for the 1 dark state fluorophore. The first three rows show the images set to the same contrast for each labeled method. The last two rows show the results for the Image Error and the percent error in the number of fluorophores for each of the three systems for the one dark state fluorophore. The lines are medians, box extends from 25% to 75%, whiskers extend to the most extreme data points not considered outliers, and the red pluses are the outliers —1.5x interquartile range

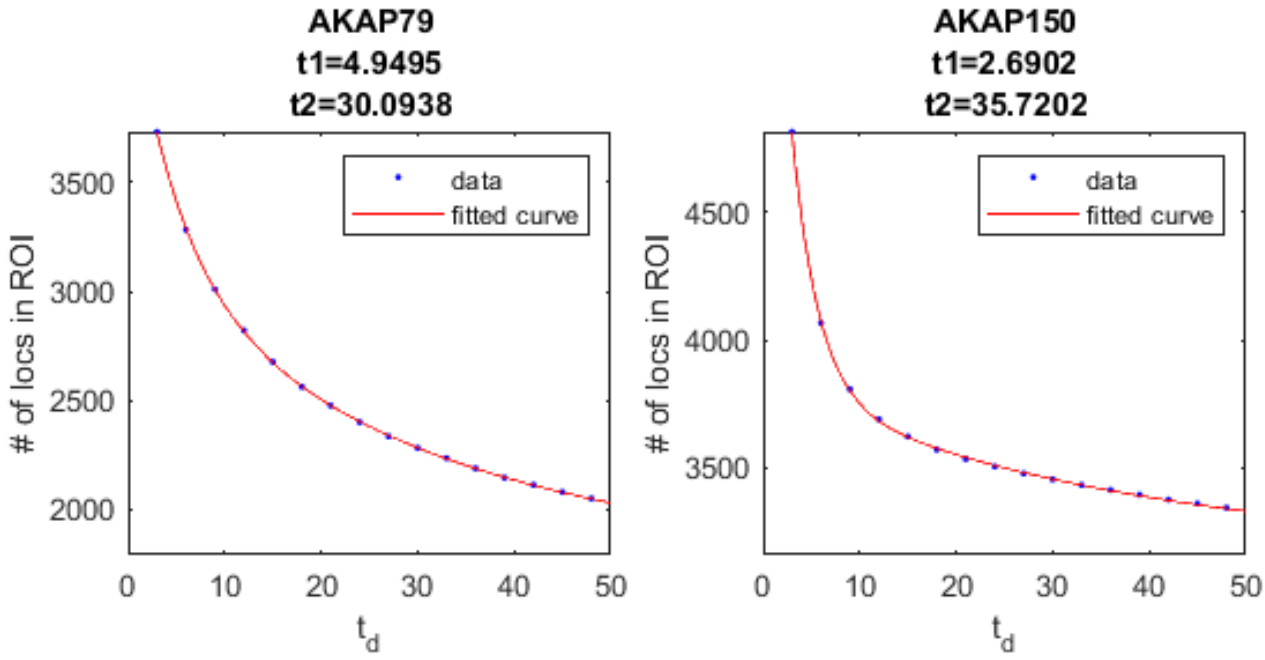

Figure S11: Here we show the results for determining the proper thresholds utilizing the methodology of T1 for AKAP79/AKAP150. The data was fitted to the double exponential used previously. Here the proper threshold is equal to two times the larger average dark time, either t1 or t2.

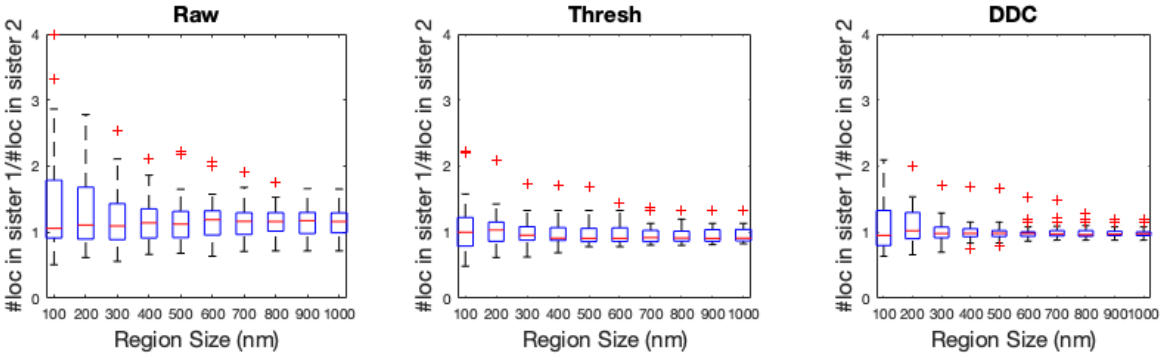

Figure S12: The ratio of the number of localizations between sister chromatids for each of the three methodologies using different sized segments along the fibers (Supporting Material, expected value is 1). The red lines are medians, box extends from 25% to 75%, whiskers extend to the most extreme data points not considered outliers, and the red pluses are the outliers —1.5x interquartile range

References

[1] Betzig, E., G. H. Patterson, R. Sougrat, O. W. Lindwasser, S. Olenych, J. S. Bonifacino, M. W. Davidson, J. Lippincott-Schwartz, and H. F. Hess, 2006. Imaging intracellular fluorescent proteins at nanometer resolution. Science 313:1642–1645.

[2] Annibale, P., S. Vanni, M. Scarselli, U. Rothlisberger, and A. Radenovic, 2011. Quantitative Photo Activated Localization Microscopy: Unraveling the Effects of Photoblinking. PLoS ONE 6:e22678–8.

[3] Coltharp, C., R. P. Kessler, and J. Xiao, 2012. Accurate Construction of Photoactivated Localization Microscopy (PALM) Images for Quantitative Measurements. PLoS ONE 7:e51725–16.

[4] Mo, G. C. H., B. Ross, F. Hertel, P. Manna, X. Yang, E. Greenwald, C. Booth, A. M. Plummer, B. Tenner, Z. Chen, Y. Wang, E. J. Kennedy, P. A. Cole, K. G. Fleming, A. Palmer, R. Jimenez, J. Xiao, P. Dedecker, and J. Zhang, 2017. Genetically encoded biosensors for visualizing live-cell biochemical activity at super-resolution. Nature Methods 14:427–434.

[5] Rossy, J., D. M. Owen, D. J. Williamson, Z. Yang, and K. Gaus, 2013. Conformational states of the kinase Lck regulate clustering in early T cell signaling. Nature Immunology 14:82–89, ISSN 15292908, doi:10.1038/ni.2488.

[6] Puchner, E. M., J. M. Walter, R. Kasper, B. Huang, and W. A. Lim, 2013. Counting molecules in single organelles with superresolution microscopy allows tracking of the endosome maturation trajectory. Proceedings of the National Academy of Sciences of the United States of America 110:16015–16020.

[7] Thevathasan, J. V., M. Kahnwald, K. Cieśliński, P. Hoess, S. K. Peneti, M. Reitberger, D. Heid, K. C. Kasuba, S. J. Hoerner, Y. Li, Y. L. Wu, M. Mund, U. Matti, P. M. Pereira, R. Henriques, B. Nijmeijer, M. Kueblbeck, V. J. Sabinina, J. Ellenberg, and J. Ries, 2019. Nuclear pores as versatile reference standards for quantitative superresolution microscopy. Nature Methods 16:1045–1053, ISSN 15487105, doi:10.1038/s41592-019-0574-9.

[8] Weng, X., C. Bohrer, K. Bettridge, A. Lagda, C. Cagliero, D. Jin, and J. Xiao, 2019. Spatial organization of RNA polymerase and its relationship with transcription in Escherichia coli. Proceedings of the National Academy of Sciences of the United States of America 116, ISSN 10916490, doi:10.1073/pnas.1903968116.

[9] Dempsey, G. T., J. C. Vaughan, K. H. Chen, M. Bates, and X. Zhuang, 2011. Evaluation of fluorophores for optimal performance in localization-based super-resolution imaging. Nature Methods 8:1027–1036.

[10] Goossen-Schmidt, N. C., M. Schnieder, J. Hüve, and J. Klingauf, 2020. Switching behaviour of dSTORM dyes in glycerol-containing buffer. Scientific Reports 10:1–8, ISSN 20452322, doi:10.1038/s41598-020-70335-0.

[11] Hirvonen, L. M. and S. Cox, 2018. STORM without enzymatic oxygen scavenging for correlative atomic force and fluorescence superresolution microscopy. Methods and Applications in Fluorescence 6, ISSN 20506120, doi:10.1088/2050-6120/aad018.

[12] Spahn, C., F. Herrmannsdörfer, T. Kuner, and M. Heilemann, 2016. Temporal accumulation analysis provides simplified artifact-free analysis of membrane-protein nanoclusters. Nature Methods 13:963–964.

[13] Lee, S. H., J. Y. Shin, A. Lee, and C. Bustamante, 2012. Counting single photoactivatable fluorescent molecules by photoactivated localization microscopy (PALM). Proceedings of the National Academy of Sciences of the United States of America 109:17436–17441, ISSN 00278424, doi: 10.1073/pnas.1215175109.

[14] Rollins, G. C., J. Y. Shin, C. Bustamante, and S. Pressé, 2015. Stochastic approach to the molecular counting problem in superresolution microscopy. Proceedings of the National Academy of Sciences of the United States of America 112:E110–8.

[15] Datsenko, K. A. and B. L. Wanner, 2000. One-step inactivation of chromosomal genes in Escherichia coli K-12 using PCR products. Proceedings of the National Academy of Sciences 97:6640–6645.

[16] Hensel, Z., X. Fang, and J. Xiao, 2013. Single-molecule Imaging of Gene Regulation In vivo Using Cotranslational Activation by Cleavage (CoTrAC). JoVE (Journal of Visualized Experiments) :e50042.

[17] Skinner, S. O., L. A. Sepúlveda, H. Xu, and I. Golding, 2013. Measuring mRNA copy number in individual Escherichia coli cells using single-molecule fluorescent in situ hybridization. Nature Protocols 8:1100–1113.

[18] Malagon, F., 2013. RNase III is required for localization to the nucleoid of the 5' pre-rRNA leader and for optimal induction of rRNA synthesis in E. coli. RNA (New York, N.Y.) 19:1200–1207.

[19] Hensel, Z., X. Weng, A. C. Lagda, and J. Xiao, 2013. Transcription-Factor-Mediated DNA Looping Probed by High-Resolution, Single-Molecule Imaging in Live E. coli Cells. PLoS Biology 11:e1001591–17.

[20] Sage, D., H. Kirshner, T. Pengo, N. Stuurman, J. Min, S. Manley, and M. Unser, 2015. Quantitative evaluation of software packages for single-molecule localization microscopy. Nature Methods 12:717–724.

[21] McKnight, S. L. and O. L. Miller Jr., 1977. Electron microscopic analysis of chromatin replication in the cellular blastoderm drosophila melanogaster embryo. Cell 12:795–804.

[22] Cella Zanacchi, F., C. Manzo, R. Magrassi, N. D. Derr, and M. Lakadamyali, 2019. Quantifying Protein Copy Number in Super Resolution Using an Imaging-Invariant Calibration. Biophysj 116:2195–2203.

[23] Lyu, Z., C. Coltharp, X. Yang, and J. Xiao, 2016. Influence of FtsZ GTPase activity and concentration on nanoscale Z-ring structure in vivorevealed by three-dimensional Superresolution imaging. Biopolymers 105:725–734.

[24] Yang, X., Z. Lyu, A. Miguel, R. McQuillen, K. C. Huang, and J. Xiao, 2017. GTPase activity-coupled treadmilling of the bacterial tubulin FtsZ organizes septal cell wall synthesis. Science 355:744–747.

[25] Nahidiazar, L., A. V. Agronskaia, J. Broertjes, B. van den Broek, and K. Jalink, 2016. Optimizing Imaging Conditions for Demanding Multi-Color Super Resolution Localization Microscopy. PLoS ONE 11:e0158884.

[26] Schneider, C. A., W. S. Rasband, K. E. N. methods, and 2012. NIH Image to ImageJ: 25 years of image analysis. nature.com .

[27] Ovesný, M., P. Křížek, J. Borkovec, Z. Svindrych, and G. M. Hagen, 2014. ThunderSTORM: a comprehensive ImageJ plug-in for PALM and STORM data analysis and super-resolution imaging. Bioinformatics (Oxford, England) 30:2389–2390.